Journal Name

COMMUNICATION

A Flexible Smart Membrane Consisting of GO Composite Fibres and Upconversion MSNs for microRNA Detection

Tongxu Gu [a], Zhaohui Ren [a], Xiang Li *[a] , Jie Huang [b] and Gaorong Han [a]

Received 00th January 20xx,
Accepted 00th January 20xx

DOI: 10.1039/x0xx00000x

www.rsc.org/

We have developed a photoluminscent membrane for microRNA detection, consisting of chemically modified mesoporous silica nanoparticles (CaF_2:Yb/Ho@MSNs) attached, via single strand DNA probes, to flexible polyurethane fibres coated with graphene oxide (GO). By detecting the release of the luminescent nanoparticles resulting from complementary co-hybridization between target miRNA sequences and the DNA probe, accurate measurements of miRNA concentration at high sensitivity levels can be obtained. The constructs therefore offer a route to rapid detection and the potential for early cancer diagnosis.

The dysregulation of microRNAs (miRNAs) is linked closely with the pathogenesis of various diseases[1-2] and hence detection of miRNAs has recently developed as an important field of research[3-4]. miR-21, which is expressed in mammalian cells, has been reported to be associated with some types of cancer[5-6] and consequently has been explored in diagnosis strategies[7]. However, the ability to rapidly and accurately detect miRNAs has remained an elusive goal. Conventional approaches for miR-21 detection can be time-consuming and experience-dependent which may make them unaffordable and inaccessible for point-of-care testing applications[8-9]. To obviate these issues alternative, novel approaches based on electrochemical sensing using multichannel screen-printed electrode arrays[10], chemiluminescence[11] and nanoparticle-based colorimetry[12] have been developed which offer inherent advantages including speed, cost-effectiveness, simplicity, and the potential for miniaturization.

While two-dimensional fluorescent membranes, have been prepared successfully in the past[13], the three-dimensional network structure of electrospun nanofibres provides the potential to increase sensitivity[14]. The combination of electrospun nanofibers and UCNPs has been considered as a promising approach for constructing fluorescent membranes for accurate miR-21 detection[15]. In comparison with current photoluminescent systems such as quantum dots and organic fluorescence molecules, upconversion nanoparticles (UCNPs) offer marked advantages, such as sharp and adjustable emission bands, high resistance to photobleaching, reduction in photoblinking, and low levels of background autofluorescence from biological systems[16].

In general, for detection systems consisting of fluorescent membranes, a photo-quencher is needed. Graphene oxide (GO) has been reported as a material with currently the highest photo-quenching effect[17]. Graphene oxide been shown to interact with single-stranded oligonucleotides via π-π stacking interactions with nucleobases[18-19]. However, the interaction

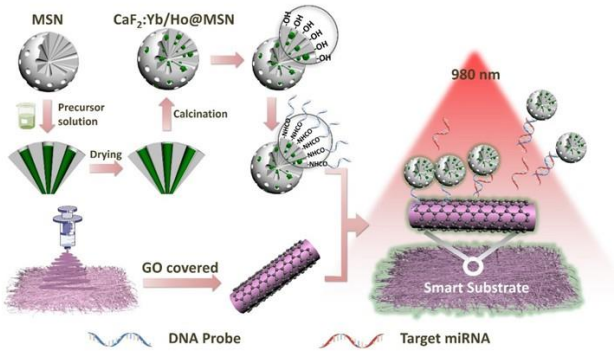

Fig. 1 Schematic illustration of the synthesis of biosensing membrane and miRNA detection.

[a] State Key Laboratory of Silicon Materials, School of Materials Science and Engineering, Zhejiang University, Hangzhou, Zhejiang 310027, People's Republic of China. E-mail: xiang.li@zju.edu.cn; Fax/Tel: +86-0571-88276240
[b] Department of Mechanical Engineering, University College London, Torrington Place, London WC1E 7JE, UK

† Electronic Supplementary Information (ESI) available: Structure parameters of MSN and CaF_2: Yb/Ho@MSN. Elemental mapping of CaF_2: Yb/Ho@MSN. TEM image of Go film. Optical photograph of TPU fibre membrane before and after GO covered. FTIR spectra of CaF_2: Yb/Ho@MSN before and after amino modification. UV-vis absorption of CaF_2: Yb/Ho@MSN modified with DNA probe. Relationship between UCL relative intensity and the concentration of miR-21 at 540 nm and 647 nm. Mir-21 detection property of the smart membrane in 10 vol% fetal bovine serum. See DOI: 10.1039/x0xx00000x

between oligonucleotides and GO weakens on the formation of double-stranded DNA through a mechanism of base complementary pairing[19]. Therefore, it has been suggested that the coupling characteristics between GO and single-stranded DNA (ssDNA) offer opportunities to develop high performance biosensing platforms[20].

In our previous studies[21, 22], we developed an upconversion inorganic electrospun fibrous membrane for miRNA detection. However, the poor capacity of inorganic materials to resist mechanical impact and their low tensile strength, limit the detection accuracy and stability. The highest limit of detection (LOD) only reached 2 nM in deionized water. Therefore, herein, we have investigated whether more accurate miRNA detection might be achieved via the development of a composite membrane, consisting of thermoplastic polyurethane (TPU)@GO electrospun fibres and high surface area upconversion mesoporous silica nanoparticles (MSNs). Additionally, the interlaced network of electrospun TPU fibres, shows both excellent stability in aqueous solution and also high affinity with GO. This combination offers a matrix with the potential for capillary-action to retain small-volume substances.

A mechanism is hypothesized in Fig. 1, the synthesis of CaF_2: Yb/Ho@MSNs involves infiltration of precursor solution by capillary effect and followed by the nucleation and growth of CaF_2: Yb/Ho nanocrystals through thermo-decomposition method. The CaF_2: Yb/Ho@MSNs synthesized with amorphous shell do not only present uniform morphology, but also show high specific surface area and large pore volume, providing sufficient space and abundant active groups for subsequent surface modification. The composite membranes are formed by the grafting of CaF_2: Yb/Ho@MSNs to GO composite fibres via a single strand DNA probe. In the presence of target miRNA, the complementary co-hybridization between the target sequence and the DNA probe causes the release of upconversion MSNs from the membrane. Upconversion luminescence intensity of the membrane can therefore be employed to quantify the concentration of miRNA.

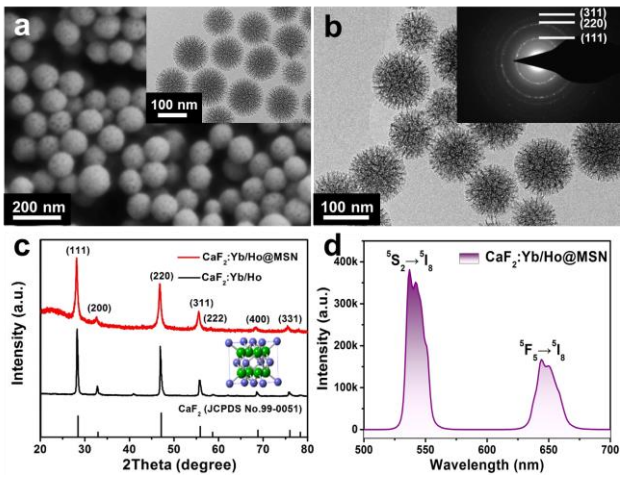

Fig. 2 (a) SEM and TEM images of MSNs. (b) TEM and SAED images of CaF_2: Yb/Ho@MSNs. (c) XRD pattern of pure CaF_2: Yb/Ho and CaF_2: Yb/Ho @MSNs. (d) UC emission spectra of CaF_2: Yb/Ho@MSNs excited at 980nm.

MSNs with radical-form pore structures, serving as a carrier for upconversion nanocrystals, were synthesized by an organic template method[24]. Transmission electron microscopy (TEM) and scanning electron microscopy (SEM) images show that the particles have a diameter of ~110 nm and a high degree of monodispersity (Fig. 2a). The precursor solution containing Ca^{2+}, Yb^{3+} and Ho^{3+} was taken up into the mesopores via capillary action. The CaF_2: Yb/Ho nanocrystals nucleated and formed in-situ within the pores by a thermal-decomposition reaction. MSNs combined with upconversion nanocrystals were darker in the TEM images (Fig. 2b), and their corresponding chemical composition was confirmed by elemental mapping of Ca, Si, O, Yb and Ho (Fig. S1, ESI†). Selected area electron diffraction (SAED) patterns (Fig. 2b, inset), indicated that CaF_2:Yb/Ho@MSNs exhibited distinct diffraction rings, attributable to the (111), (220), (311) reflections of the CaF_2 cubic phase (JCPDS no.99-0051). The X-Ray diffraction (XRD) pattern was in good agreement with the SAED pattern, verifying the presence of cubic CaF_2 nanocrystals within the CaF_2:Yb/Ho@MSNs obtained (Fig. 2c). The Brunauer-Emmett-Teller surface area of MSNs and CaF_2: Yb/Ho@MSNs were measured to be ~747 $m^2\ g^{-1}$ and ~454 $m^2\ g^{-1}$, respectively (Table S1). The average pore diameter did not vary significantly before and after upconversion nanocrystals had been embedded in the fibres according to the nitrogen adsorption-desorption isotherm and corresponding pore-size distribution. The unique radical-form porous structure offered a favourable substrate for the subsequent surface modification and functionalization. As shown in Fig. 2d, the upconversion MSNs showed two main emission bands at 540 nm and 647 nm under irradiation using a 980 nm laser. This corresponded to an energy-transfer process from the excited states $^5S_2$ and $^5F_5$, respectively, to the ground state $^5I_8$, similar to that of Yb/Ho co-doped upconversion materials reported previously[25].

TPU fibres used as a flexible substrate were synthesized via an electrospinning process. The membrane network consisted of uniform TPU fibres with a smooth surface and random orientation (Fig. 3a). After immersing in GO aqueous solution, the TPU fibres were covered with a hydrogen-bonded layer of GO flakes[40]. The presence of the coating was verified using high magnification SEM images (Fig. 3b). The GO coating was extremely thin with a smooth, mat-like surface morphology and this was investigated by TEM (Fig. S2, ESI†). The GO coating resulted in the TPU@GO constructs having a grey-black appearance (Fig. S3, ESI†). Examination using Raman spectroscopy showed that pure GO and TPU@GO composite fibres exhibited a typical D-band peak ~1350 cm^{-1} and a G-band peak ~1580 cm^{-1}, corresponding to the sp^2 and sp^3 carbon stretching modes (Fig. 3c). The findings above indicated that the surfaces of the TPU fibres were successfully decorated with GO.

CaF_2: Yb/Ho@MSNs were functionalized with amino groups by amino-propyltriethoxy-silane (APTES) to provide anchoring sites (carboxyl groups) for the DNA probe. Fourier transform infrared spectroscopy (FTIR) was conducted to study the surface modification of amino groups. As shown in Fig. S4 (ESI†), a new peak at 1560 cm^{-1} was detected and identified as the bending vibration of N-H bond. The DNA probe used was complementary to the target miR-21, and it was modified with carboxyl group at the 5' end prior to its usage (Table 1). The DNA probes were covalently conjugated to the amino modified CaF_2: Yb/Ho@MSNs using EDC/NHS coupling under gentle shaking at 37°C. Compared with the UV-vis spectra of CaF_2: Yb, Ho@MSNs-NH_2, the CaF_2: Yb/Ho@MSNs conjugated DNA probe exhibited a new absorption band centred at ~258 nm, corresponding to the characteristic absorption band of DNA (Fig. S5, ESI†). The probe grafting was further verified by ζ-potential measurements, as compared with the surface charge of CaF_2: Yb/Ho@MSNs. Fig. S6 (ESI†) indicates that the as-synthesized CaF_2: Yb/Ho@MSNs had a negative charge of -13±1.7 mV. After functionalization with amino groups, the surface of CaF_2: Yb/Ho@MSNs became positively charged (8.5±2.7 mV). The ζ-potential reversed after conjugating with DNA probe at -1.1±1.5 mV. Subsequently, the smart membrane was constructed by mixing the DNA probe decorated CaF_2: Yb/Ho@MSNs and GO composite fibres by gentle shaking at room temperature. It has been reported that GO interacts strongly with ssDNA through π-π stacking between the aromatic hexagonal lattice of GO and the ring structure from the nucleotide bases. The adsorption of double-stranded DNA (dsDNA) onto the GO sheets is hampered due to shielding of the nucleobases by the negative charges from the phosphate backbone[26, 27]. Therefore, the surface of TPU@GO composite fibres show particular affinity toward ssDNA. In consequence, after immersion, a uniform coverage of CaF_2: Yb/Ho@MSNs on the surface of GO composite fibres was achieved, as shown in Fig. 3d.

The detection performance of this flexible smart membrane was studied using solutions containing at target miR-21 with different concentration. As shown in Fig. 4a, the intensity of upconversion luminescence, at 540 nm and 647 nm, gradually decreased with increasing miRNA over a wide range from 1 pM to 100 μM. The relationship between relative photoluminescence intensity and the concentration of miR-21

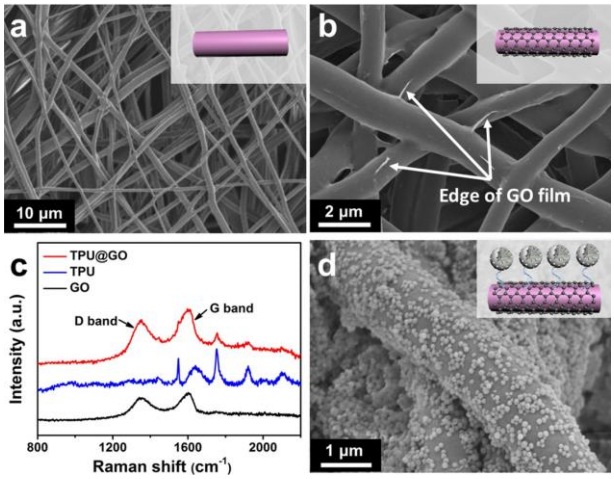

Fig. 3 SEM image of (a) as-prepared TPU fibres and (b) TPU@GO composite fibres. (c) Raman spectra of TPU before and after GO coverage. (d) SEM images of the hybrid membrane combining with CaF_2: Yb/Ho@MSN-probe and TPU@GO composite fibres.

is shown in Fig. S7 (ESI†). Over the miR-21 concentration range 20 pM~1 μM, there was a linear relationship with the relative photoluminescence at 540 nm and 647 nm and a correlation coefficient $R^2 > 0.99$ (Fig. 4b and c). In the presence of miR-21, the interaction between the single-stranded oligonucleotides and GO weakened, owing to the formation of double-stranded DNA. This caused the liberation of nanoparticles from the GO substrate and these observations agree well with the phenomena reported in previous studies[28, 29]. In consequence, a clear relationship between the photoluminescence of the composite membrane and miR-21 concentration was achieved down to a detection limit of 20 pM.

In addition, the detection of miR-21 in a simulated biological condition was also assessed using a 10 vol% fetal bovine serum. When the concentration of miR-21 was increased from 2 nM to 200 μM, the UCL intensity decreased, and there was a linear relationship between miR-21 concentration and the intensity of UCL peaks at both 540 nm and 647 nm, indicating a detection limit of 2 nM (Fig. S8, ESI†). The reduction in on upconversion emission and miRNA detection performance in serum, can be

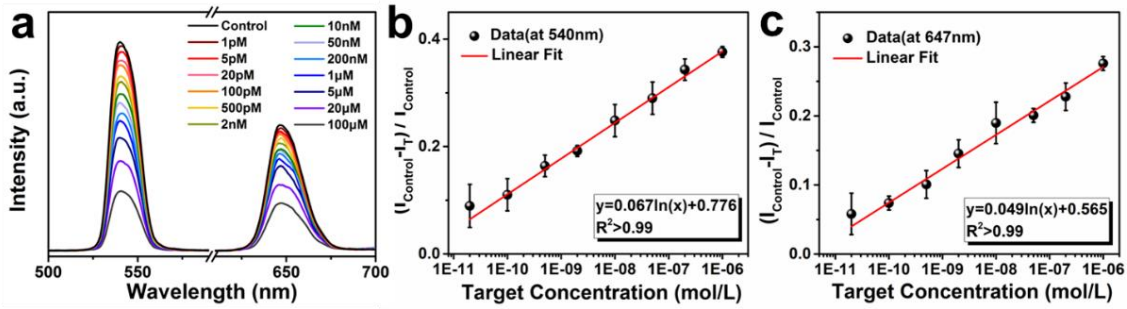

Fig. 4 (a) UCL spectra of the smart membrane after treating with solutions with different miR-21 concentration, and the relationship between the relative intensity of UCL, at (b) 540 nm and (c) 647 nm, and miR-21 concentration at a certain range.

Table 1 Oligonucleotide sequences used in miRNA detection.

Oligonucleotide Name	Sequence (5'-3')
miR-21	UAGCUUAUCAGACUGAUGUUGA
anti-miR-21	COOH-TCAACATCAGTCTGATAAGCTA
mismatch-1	UAGCUUAUCCGACUGAUGUUGA
mismatch-2	UAGCUUAUACUACUGAUGUUGA
miR-195	UAGCAGCACAGAAAUAUUGGC

attributed to the adsorption of protein molecules. To further demonstrate the detection specificity of the composite membrane, miR-21 with single-base mismatch and three-base mismatch were used as close-related targets, and miR-195, another common breast-cancer biomarker, was selected as an irrelevant target, as listed in Table 1. As shown in Fig. S9 (ESI†), in the presence of 1 μM miR-195, miR-21 with single-base and three-base mismatch respectively, the UCL intensity of the membrane did not present clear difference comparing to the blank control. In contrast, when the same concentration of miR-21 was added, the UCL intensity decreased significantly. The corresponding variation of UCL intensity at 540 nm and 647 nm were summarized in Fig. S9b&c (ESI†), indicating the potential of the composite membrane in specific detection of target microRNA.

In summary, a smart membrane consisting of upconversion MSNs and GO composite fibres was designed and synthesized for miRNA detection. In this system, the upconversion MSNs, synthesized by an in-situ nanocrystalline growth method, showed high specific area and abundant active groups, which were favourable for modification via DNA probes. The electrospun TPU fibres were used as a substrate which, when combined with a GO coating, shows strong affinity toward single-stranded oligonucleotides conjugated with upconversion MSNs. In the presence of target miRNA, the complementary interaction between the DNA probe and miRNA resulted in detachment of upconversion MSNs from the membrane, and a consequent reduction in UCL intensity. This provided quantitative miRNA detection with a limit of 20 pM. The interlaced network of the membrane showed strong-capillary-action and hence enrichment effects, which improved the accuracy of miRNA detection. This flexible composite membrane therefore offers a novel approach for accurate miRNA detection and has potential for application in early cancer diagnosis.

This work was financially supported by the National Nature Science Foundation of China (51672247), the '111' Program funded by Education Ministry of China and State Administration of Foreign Experts Affairs (B16043).

Conflicts of interest

There are no conflicts to declare.

Notes and references

1 D. P. Bartel, *Cell*, 2004, **116**, 281-297.
2 V. Ambros, *Nature*, 2004, **431**, 350-355.
3 S. M. Hammond, *Adv. Drug Deliv. Rev.*, 2015, **87**, 3-14.
4 M. S. Nicoloso, R. Spizzo, M. Shimizu, S. Rossi and G. A. Calin, *Nat. Rev. Cancer* 2009, **9**, 293-302.
5 P. S. Mitchell, R. K. Parkin, E. M. Kroh, B. R. Fritz, S. K. Wyman, E. L. Pogosova-Agadjanyan, A. Peterson, J. Noteboom, K. C. O'Briant, A. Allen, D. W. Lin, N. Urban, C. W. Drescher, B. S. Knudsen, D. L. Stirewalt, R. Gentleman, R. L. Vessella, P. S. Nelson, D. B. Martin and M. Tewari, *PNAS*, 2008, **105**, 10513-10518.
6 L.Yan, X. Huang, Q. Shao, M. Huang, L. Deng, Q. Wu, Y. Zeng and J. Shao, *RNA*, 2008, **14**, 2348-2360.
7 R. Kumarswamy, I. Volkmann and T. Thum, *RNA biology*, 2011, **8**, 706-713.
8 A. Válóczi, C. Hornyik, N. Varga, J. Burgyán, S. Kauppinen and Z. Havelda, *Nucleic Acids Res.*, **32**, e175.
9 C. C. Pritchard, H. H. Cheng and M. Tewari, *Nat. Rev. Genet.*, 2012, **13**, 358-369.
10 A. Erdem, G. Congur and E. Eskin, *Sensor Actuat. B-Chem.*, 2013, **188**, 1089-1095.
11 S. Bi, J. Zhang, S. Hao, C. Ding and S. Zhang, *Anal. Chem.*, 2011, **83**, 3696-3702.
12 W. Yang, X. Li, Y. Li, Li. Zhao, W. He, Y. Gao, Y. Wan, W. Xia, T. Chen, H. Zheng, M. Li and S. Xu, *Anal. Biochem.*, 2008, **376**, 183-188.
13 W. Guan, W. Zhou, J. Lu and C. Lu, *Chem. Soc. Rev.*, 2015, **44**, 6981-7009.
14 X. Wang, C. Drew, S. Lee, K. J. Senecal, J. Kumar and L. A. Samuelson, *Nano Lett.*, 2002, **2**, 1273-1275.
15 L. Wang, R. Yan, Z. Huo, L. Wang, J. Zeng, J. Bao, X. Wang, Q. Peng and Y. Li, *Angew. Chem, Int. Ed.*, 2005, **44**, 6054-6057.
16 F. Wang, D. Banerjee, Y. Liu, X. Chen and X. Liu, *Analyst*, 2010, **135**, 1839-1854.
17 Y. He, X. Xing, H. Tang and D. Pang, *Small*, 2013, **9**, 2097-2101
18 C. Lu, H. Yang, C. Zhu, X. Chen and G. Chen, *Angew. Chem, Int. Ed.*, 2009, **48**, 4785-4787.
19 C. Liu, Z. Wang, H. Jia and Z. Li, *Chem. Commun.*, 2011, **47**, 4661-4663
20 H. Dong, J. Zhang, H. Ju, H. Lu, S. Wang, S. Jin, K. Hao, H. Du and X. Zhang, *Anal. Chem.*, 2012, **84**, 4587-4593.
21 Y. Fu, T. Chen, G. Wang, T. Gu, C. Xie, J. Huang, X. Li, S. Best and G. Han, *J. Mater. Chem. B*, 2017, **5**, 7133-7139.
22 G. Wang, Y. Fu, Z. Ren, J. Huang, S. Best, X. Li and G. Han, *Chem. Commun.*, 2018, **54**, 6324- 6327.
23 T. Gu, L. Cheng, F. Gong, J. Xu, X. Li, G. Han and Z. Liu, *ACS Appl. Mater. Interfaces*, 2018, **10**, 15494-15503.
24 A. Nandiyanto, S. Kim, F. Iskandar and K. Okuyama, *Microporous Mesoporous Mater.*, 2009, **120**, 447-453.
25 G. Ren, S. Zeng and J. Hao, *J. Phys. Chem. C*, 2011, **115**, 20141-20147.
26 A. Wojcik and P. V. Kamat, *ACS Nano*, 2010, **4**, 6697-6706.
27 H. Wang, T. Chen, S. Wu, X. Chu and R. Yu, *Biosens. Bioelectron.*, 2012, **34**, 88-93.
28 C. Liu, Z. Wang, H. Jia and Z. Li, *Chem. Commun.*, 2011, **47**, 4661-4663.
29 D. Giust, M. I. Lucío, A. H. El-Sagheer, T. Brown, L. E. Williams, O. L. Muskens and A. G. Kanaras, *ACS nano*, 2018, **12**, 6273-6279.

Please do not adjust margins